The Astrophysical Journal, 653:1342–1352, 2006 December 20


# THE EXCITATION OF SO IN COLD MOLECULAR CLOUDS: TMC-1

F. Lique
LERMA and UMR 8112 du CNRS, Observatoire de Meudon, F-92195 Meudon Cedex, France; francois.lique@obspm.fr

J. Cernicharo
DAMIR, IEM-CSIC, Calle Serrano 121, E-28006 Madrid, Spain; cerni@damir.iem.csic.es

and

P. Cox
IRAM, 300 rue de la Piscine, F-38406 Saint-Martin-d'Hères, France; cox@iram.fr
*Received 2006 April 19; accepted 2006 September 3*

## ABSTRACT

We have performed calculations on the excitation of SO using the accurate collisional rate coefficients at low temperatures for the system SO-He recently published by Lique et al. Compared with the results of Green, the new excitation rates show significant differences for transitions involving the low energy levels. We present a set of radiative transfer models for different cloud geometries and physical conditions, using the new rate coefficients for SO, and show that they provide a more correct diagnostic of the physical conditions of cold dark clouds. We have applied these results to observations of mapping results in TMC-1 done in the $2_3$–$1_2$, $3_4$–$2_3$, and $2_2$–$1_1$ transitions (using the IRAM 30 m telescope) and the $0_1$–$1_0$ transition (using the 100 m Effelsberg radio telescope). The intensity maxima for all these lines is found around the so-called ammonia peak. The structure of TMC-1 is well represented by a cylindric filament with several cores [$T_K = 8$ K, $n(\mathrm{H_2}) \sim 3 \times 10^4$ cm$^{-3}$] surrounded by an envelope [$T_K = 10$ K, $n(\mathrm{H_2}) \sim (6\text{–}8) \times 10^3$ cm$^{-3}$] showing a complex velocity structure. The abundance of SO in TMC-1 is nearly constant along the filament, $X(\mathrm{SO}) \simeq 10^{-8}$, except at the ammonia peak, where a higher SO abundance, $X(\mathrm{SO}) \simeq 2.5 \times 10^{-8}$, is required.

*Subject headings:* ISM: abundances — ISM: individual (TMC-1) — ISM: molecules — molecular processes

*Online material:* color figures

## 1. INTRODUCTION

The observation of molecular emission at millimeter and infrared wavelengths, supplemented by careful and detailed modeling, is a powerful tool for investigating the physical and chemical conditions of astrophysical objects. First observed by Gottlieb & Ball (1973) in the interstellar gas, sulfur monoxide has been used extensively to study molecular gas in various environments such as dark clouds, warm molecular clouds, evolved stars, or shocks (Turner et al. 1992; van Dishoeck et al. 1993; Blake et al. 1987; Pineau des Forêts et al. 1993). SO is a good probe since the fine structure in its $^3\Sigma^-$ electronic ground state gives many relatively close transitions. Its dipole moment, 1.55 D, allows one to trace regions of different densities by selective rotational transitions of increasing Einstein coefficients.

In regions of star formation (high and low mass), the outflows from the young stars penetrate the surrounding envelopes and thus create high-temperature shocks, leading to evaporation of dust mantles that produce many species in the gas phase. These freshly evaporated molecules can then drive a rich and complex chemistry, specific to the physical conditions present in the gas. In particular, the observed abundances of the sulfur-bearing molecules in the warm gas display important differences from those derived from observations of cold molecular material. They also exhibit large abundance gradients on small spatial scales. In these warm clouds, the sulfur is originally contained in $H_2S$, which reacts with hydrogen atoms to give sulfur atoms that rapidly react with OH, $O_2$, and O to form SO, $SO_2$, and other sulfur-bearing species. Because of the relatively fast evolution of their chemistry on timescales of the hot-core age, the warm gas can be traced with molecules such as SO and $SO_2$ (Turner et al. 1992; van Dishoeck et al. 1993; Blake et al. 1994). Nevertheless, SO is also present at large scales in the cold parental gas surrounding the newly formed stars. This complexity renders the determination of abundances of sulfur-bearing molecules difficult, and the study of the chemical evolution of the gas needs to be done through a detailed analysis of the molecular emission that arises from regions of very different temperatures and densities.

Detailed calculations for the collisional rates of SO with He and/or $H_2$ do not exist. Excitation rate coefficients for collision among fine-structure levels of SO with $H_2$ were provided some time ago by Green (1994, hereafter G94), using coupled states and recoupling approximations to collision dynamics. These calculations were based on a potential energy surface (PES) obtained for CS-He using an electron-gas model and modified for long-range interaction to simulate a CS-$H_2$ PES (Green & Chapman 1978). These collisional rates are rather uncertain since the used PES was adapted from the CS-He system, which is different from the PES for the SO-He system. Indeed, the comparison of the surfaces of the two systems obtained by accurate ab initio quantum chemistry calculations shows large differences between them, in particular for the position and the depth of the well (Lique et al. 2006). New accurate rate coefficients among fine-structure levels of SO were calculated recently (Lique et al. 2005, hereafter L05), using the full close coupling method for temperatures ranging from 5 to 50 K. Large difference of up to a factor 10 exist between these new results and the previous results reported by G94.

In this paper, we analyze the impact of the new rates on the excitation of SO by modeling the pumping of its rotational energy levels through LVG (large velocity gradient) and nonlocal radiative transfer models. We have selected in our calculations a wide range of physical conditions. These calculations are used to

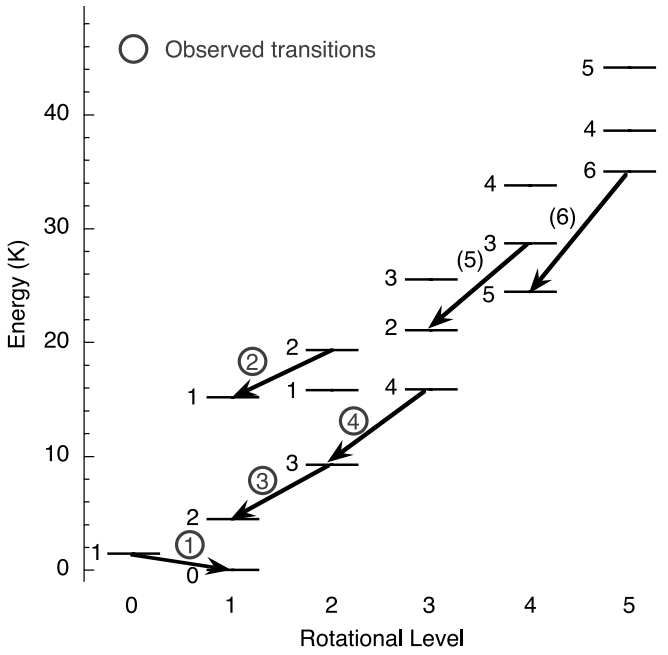


FIG. 1.—Diagram of the energy levels of SO. [*See the electronic edition of the Journal for a color version of this figure.*]

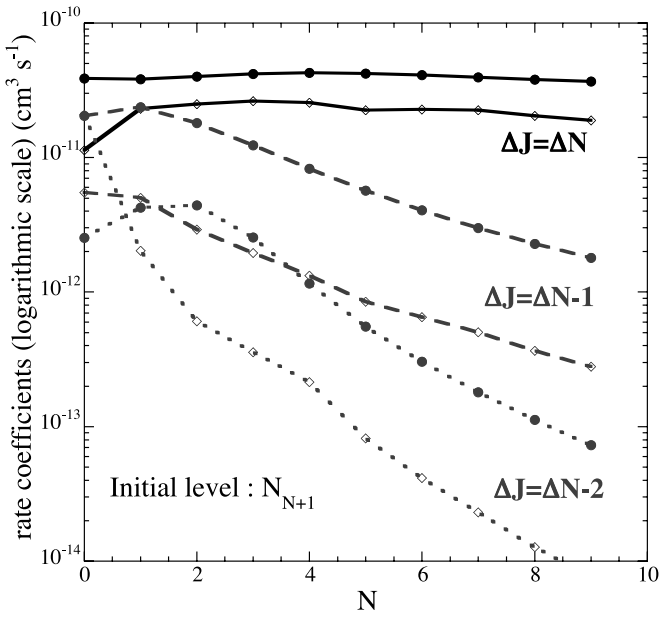


FIG. 2.—L05 SO collisional rates at 50 K (*filled circles*) compared to those of G94 (*open diamonds*). [*See the electronic edition of the Journal for a color version of this figure.*]

analyze mapping results obtained toward the cold molecular cloud TMC-1 in a series of transition of SO. Since the detection of $HC_3N$ in this cloud (Morris et al. 1976), TMC-1 has been the subject of many observational studies (Cernicharo et al. 1984; Cernicharo & Guélin 1987; Pratap et al. 1997; Snell et al. 1982; Avery et al. 1982), including SO observations (Rydbeck et al. 1980; Hirahara et al. 1995). In this paper, we study the influence of the new rate coefficients on the interpretation of the observations, and we provide new physical parameters for TMC-1.

## 2. MODELING

### 2.1. *Collisional Rates for* SO

In the SO ($^3\Sigma^-$) electronic ground state, the rotational levels are split by spin-rotation coupling. In the intermediate coupling scheme, the rotational wave function $|F_i jm\rangle$ are linear combinations of pure Hund's case *b* wave functions $|NSjm\rangle$. For SO, the case *b* limit becomes valid beyond $N = 5$. All collision calculations were carried out with the exact energy levels including the fine-structure interaction. However, we will use in the following the usual level labeling $N_J$ where $N = J - 1$, $N = J$, $N = J + 1$ corresponds to the $F_1$, $F_2$, and $F_3$ levels. The energies of the first fine levels of SO are shown in Figure 1.

The new rate coefficients for SO-He by L05 have been calculated for low temperature (5–50 K) using an exact close coupling method and an accurate ab initio PES. These rates are the first calculated for these low temperatures. Rate coefficients for SO in collision with $H_2(J = 0)$ can be roughly estimated from those of SO-He by using the ratio of the reduced mass of both systems. Previous calculations by G94 were done for rotational excitation of SO by collision with $H_2(J = 0)$ for temperatures ranging from 50 to 300 K. It is difficult to extrapolate these rates for the physical conditions prevailing in dark clouds. Moreover, the PES of G94 was estimated from the one calculated for CS-He using an electron-gas model and a recoupling approximation from spin-free rate coefficients, which leads to uncertainties in his rate coefficients. A comparison of the rates at 50 K (Fig. 2) shows that those obtained by G94 for SO-$H_2$, and transformed into SO-He coefficients by the ratio of reduced masses, are on average a factor of 2–3 below the recent ones for the $\Delta J = \Delta N$ transitions. However, the differences may be as large as a factor of 10 for transitions involving different selection rules. These differences will probably grow at low temperatures if Green's methods were used (see detailed discussion in L05). It could be argued that we compare different systems. However, a comparison of the CO-He and CO-$H_2$ (Green & Thaddeus 1976) collisional rates at 60 K shows that individual collisional rates, $k_{JJ'}$, are similar within a constant scale factor. We could expect a similar behavior for SO-He and SO-$H_2$ since SO is heavier than CO. Hence, the differences observed in Figure 2 are due to the different methods used for the calculations. More specifically, the precision of the PES method appears to be critical, the method used in L05 being the more accurate one.

### 2.2. *LVG Modeling*

The LVG approach, first proposed by Sobolev (1958, 1960) and further developed by Castor (1970), provides a local expression for the angle-averaged mean intensity that thoroughly simplifies the resolution of the statistical equilibrium equations. This approximation implies that the velocity gradient is large enough to decouple radiatively the different points of the cloud. For each point of the cloud the excitation conditions depend only on the local density, the kinetic temperature, and the escape probability. Rotational excitation of sulfur monoxide can be induced by collisions with $H_2$ and He, as well as by absorption of photons. Our LVG calculations treat only fine-structure levels of the ground electronic state of SO. We refer to Castor (1970) and Goldreich & Kwan (1974) for the relevant equations used in the LVG calculation of the rotational level population and excitation and brightness temperatures.

Figure 3 shows the comparison between the results obtained with the rate coefficients of L05 and those of G94. The top panel of Figure 3 compares the brightness temperature $T_B$ at $T_K =$ 10 K for several SO lines. The rate coefficients of G94 are extrapolated to 10 K (adopting a linear extrapolation to the logarithm of the rates) since the lowest temperature in the G94 calculations is

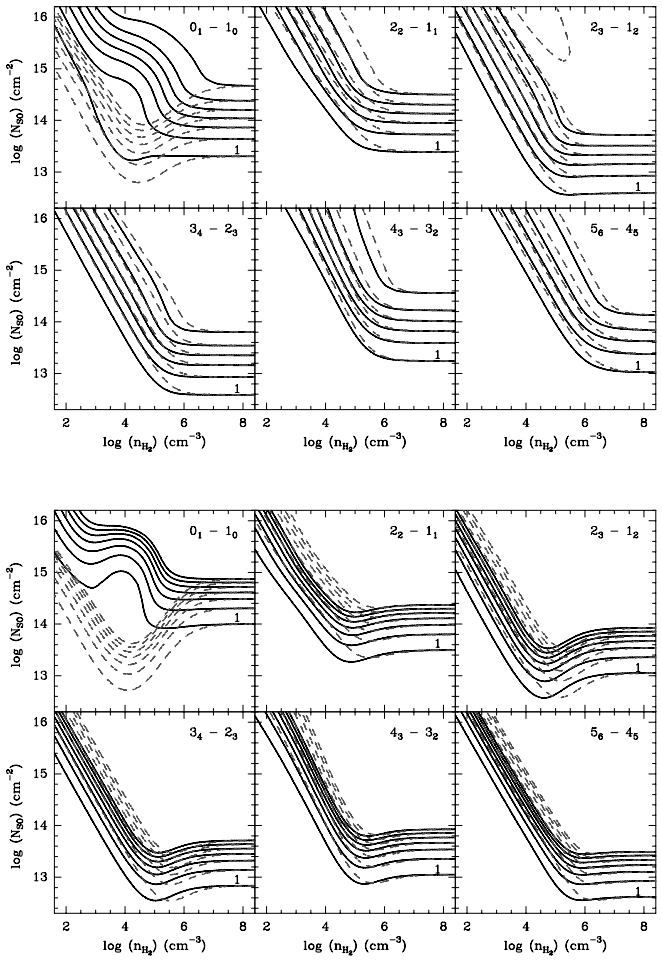


FIG. 3.—Comparison of $T_B$ using L05 (*solid curves*) and G94 (*dashed curves*) collisional rates for $T_K = 10$ K (*top*) and $T_K = 50$ K (*bottom*). The G94 rates at $T_K = 10$ K have been extrapolated from those at 50 K (see text). [*See the electronic edition of the Journal for a color version of this figure.*]

50 K. The brightness temperature $T_B$ has a similar behavior for all the transitions $\Delta J = J_u - J_l = \Delta N = N_u - N_l$ from both rate sets. It is clear from Figure 3 that for a given line intensity and volume density different column densities are obtained from the two sets of collisional rates (or different volume densities if the input parameter is the column density). Using the rates of G94, the determination of the density or the column density in cold molecular clouds will result in overestimates when compared to the results based on the L05 rates. These differences for the density and column density can reach a factor $\sim 2$–3. For the $0_1$–$1_0$ transition (see plot in top panel of Fig. 3), and more generally for all radiative transitions with $\Delta N = -1$, the results are quite different: $T_B$ has a different behavior using the two sets of rate coefficients, and especially for a given $n(H_2)$ and column density, $T_B$ is lower when the L05 rates are used. In this case, the difference in brightness temperature between both rate sets can reach a factor 10.

These results are not really surprising in view of the different methods used to obtain both sets of collisional rates and to the crude approximation adopted to extrapolate Green's rates at 10 K. This difference is due to the approximations adopted for the dynamical calculations: (1) the fact that G94 uses a pure Hund's case *b* to describe the SO energy levels, which is not well adapted to SO, especially for low energy levels; (2) the adopted recoupling method (see § 2.1), which leads to large differences (up to a factor 10) for all downward transitions with $\Delta N > 0$ (or upward transitions with $\Delta N < 0$) that are due to the incorrect description of energy levels in the approach of G94, where the fine-structure splitting of the energy levels is not taken into account in the dynamical calculations; and (3) the different PES used in the calculations. All these effects have been discussed in detail by L05. As noted above, the G94 rates are lower than those of L05 by a factor of 2–3 for $\Delta N = \Delta J$ transitions and by a factor of 10 for the other transitions (see above). The result on the collisional excitation of these transitions is that the G94 rates lead to lower excitation temperatures. Hence, the interpretation of SO observations toward dark clouds using G94 rates will result in an overestimate of the density (or the column density) by a similar factor. The $0_1$–$1_0$ transition has a different behavior, with a clear trend to understimate the density. Some previous determinations of the SO abundances in dark molecular clouds are based on the observation of this line (Rydbeck et al. 1980). The use of G94 rates will certainly produce an underestimate of the density $n(H_2)$ (or the column density) that can be as high as 1 order of magnitude. All transitions $N_N$–$(N+1)_{N-1}$ will provide a similar behavior if the G94 rates are used. This effect does not depend on the temperature and is related to the approach adopted by G94 for the dynamical calculations.

In order to check the effect on the excitation of SO of the adopted extrapolation for $T_K = 10$ K, we have made additional calculations at $T_K = 50$ K with both sets of rate coefficients. Figure 3 (*bottom*) shows the excitation temperature at $T_K = 50$ K for the same SO lines as at $T_K = 10$ K. As expected, the differences are also significant, even more than at $T_K = 10$ K. This confirms that the differences seen in Figure 3 (*top*) are not due to the extrapolation of the rate coefficients down to $T_K = 10$ K, but to the difference of both sets of rates, as discussed in the above paragraph.

Depending on the transition observed, we have seen that the interpretation of observations of SO in dark molecular clouds with G94 rates can lead to an important under- or overestimate of the density $n(H_2)$ (or the column density). Since we believe that the SO-He rate coefficients of L05 represent a better approach than those of SO-$H_2$, we recommend their use for astrophysical modeling. In the following sections we use the L05 rate coefficients. Now we will analyze our LVG results to find which transitions can be used to trace the volume density and column density of SO for the typical physical conditions prevailing in dark clouds.

For low-density regions ($<10^4$ cm$^{-3}$), Figure 3 shows that molecular clouds can be modeled through the observation of the $0_1$–$1_0$ transition since it has a low Einstein coefficient and can have a strong intensity even for small $n(H_2)$. In these regions, the intensity of lines involving high energy levels will be too weak. Unfortunately, the intensity of the $0_1$–$1_0$ line is not very sensitive to $N$(SO) due to the opacity of the line. For $N(SO) = 3 \times 10^{13}$ cm$^{-2}$, $n(H_2) = 10^4$ cm$^{-3}$, and $\Delta v = 0.3$ km s$^{-1}$, we obtain $\tau \simeq 1$ and $T_{ex} = 4.7$ K. The increase of the column density by a factor of 10 does not affect significantly the excitation temperature, and hence the expected brightness temperatures are very similar for both values of $N$(SO) (1.4 vs. 1.7 K; see the effect in the upper left plots of Fig. 3 for lower densities and different column densities). Hence, a determination of the column density of SO based only on the observation of this line and assuming a value for $T_{ex}$ will probably be uncertain. If the column density is high ($\sim 10^{14}$ cm$^{-2}$), transitions between higher energy rotational levels ($2_3$–$1_2$ and $3_4$–$2_3$) will start to be detectable and could be used to estimate $n(H_2)$ and to get better constrains on $N$(SO).

For intermediate-density regions [$10^4 < n(H_2)/\text{cm}^{-3} < 10^5$], the transitions $2_3$–$1_2$ and $3_4$–$2_3$ will be strong and could be used

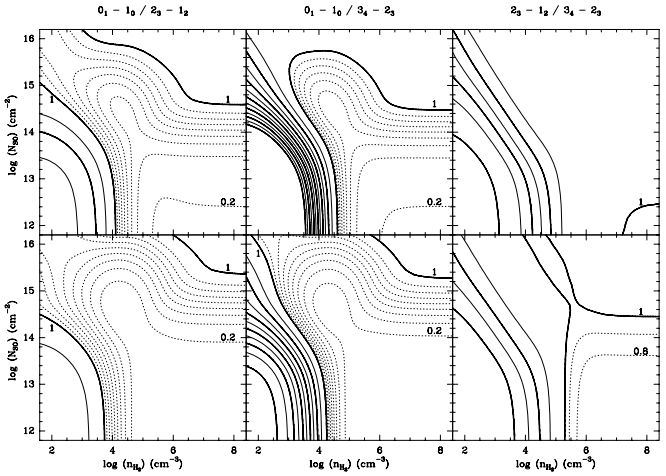


FIG. 4.—LVG line intensity ratios at 10 K (*top panels*) and 20 K (*bottom panels*) for the observed SO transitions in TMC-1.

to determine $N$(SO), whatever the $N$(SO), because the intensity of the lines is strongly coupled to the column density of SO for these densities (see upper right and lower left plots of Fig. 3). For these lines an increase of column density, for constant volume density, produces a significant increase of the excitation temperature due to radiative trapping (even if the lines are optically thick). In these regions it could be useful to observe also the $0_1$–$1_0$ transition to constrain the modeling since this line will also be very strong for these densities. Transitions between higher energy levels will be weak, except if the $N$(SO) is very high. However, it could be interesting to observe at least one of them to get a good upper limit to the volume density.

For high-density regions, the transitions between high-energy rotational levels (starting from levels higher than $N_J = 2_2$) should be a good tool for the determination of $N$(SO) and $n(H_2)$. However, large values for $N$(SO) will be needed to produce significant emission in these lines.

In order to have a quick guess for the physical conditions in dark clouds from SO observations, we have made a plot (see Fig. 4) of the brightness temperature ratio for the transitions usually observed in these objects ($0_1$–$1_0$, $2_3$–$1_2$, and $3_4$–$2_3$) and for $T_K =$ 10 and 20 K. Figure 4 shows that the intensity of the transition $0_1$–$1_0$ is lower than that of transitions $2_3$–$1_2$ and $3_4$–$2_3$ for the typical physical conditions in dark clouds. The intensity of the transitions $2_3$–$1_2$ and $3_4$–$2_3$ is similar, with the transition $2_3$–$1_2$ being slightly higher than the other. These results confirm the discussion in previous paragraphs, i.e., the $0_1$–$1_0$ transition will be strong compared to the others for low $n(H_2)$, but will become weaker than the others for higher densities and/or temperatures.

### 2.3. *Monte Carlo Models*

We have also calculated the theoretical line profiles of SO with a Monte Carlo code, very similar to that of the Monte Carlo method of Bernes (1979) but using the improvements described by Gonzalez-Alfonso & Cernicharo (1993). The cloud is assumed to be spherical and it is divided into a set of shells with homogeneous physical conditions. The number of simulated emissions (or the number of radiatively induced excitations) caused by these model photons in each shell are used to recalculate new level populations through the statistical equilibrium equations. The weight of the model photons is modified continuously to account for the absorptions occurring along their path. The process is repeated until the problem relaxes to a solution. For moderate opacities ($\tau \leq 100$), the method converges in less than 50 iterations.

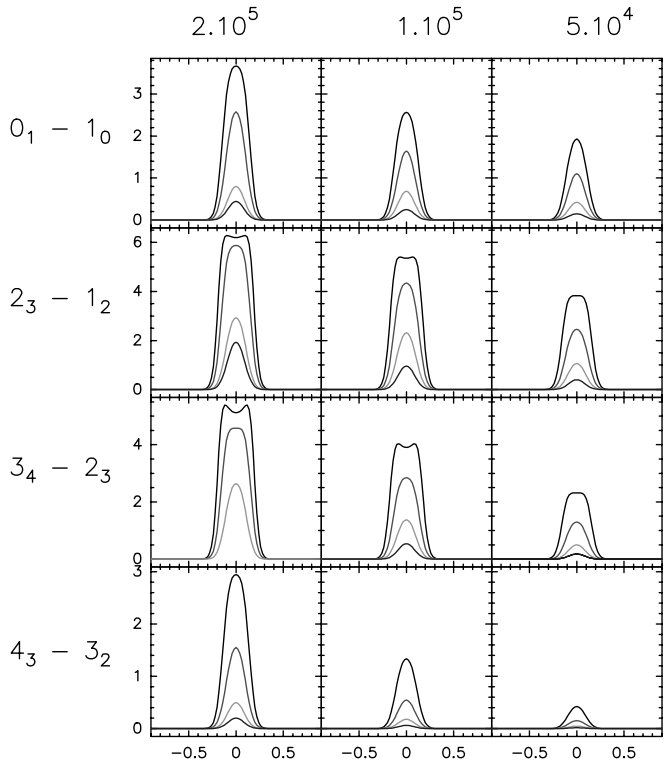


FIG. 5.—Line profiles for different SO transitions obtained with the nonlocal radiative transfer method described in the text. The cloud consists of a high-density region (core) with a diameter of 40″. Density is indicated above the panels. The cloud is placed at 140 pc. The SO abundance varies from $10^{-8}$ to $3.3 \times 10^{-10}$ in steps of $1/(10)^{1/2}$. [*See the electronic edition of the Journal for a color version of this figure.*]

We have computed models with a high-density core alone and with a low-density envelope. The parameters of the models are typical for dark clouds. For the core we have used $n(H_2) = 2 \times 10^5$, $10^5$, and $5 \times 10^4$ cm$^{-3}$, $X$(SO) $= 3.3 \times 10^{-10}$ to $10^{-8}$ in steps of 3.3, a distance of 140 pc, and a radius of 20″. For the envelope the volume density has been allowed to vary between $10^3$, $5 \times 10^3$, and $10^4$ cm$^{-3}$, and two different values for the radius, 40″ and 80″, have been used. The SO abundance in the envelope is the same than for the core in all models.

Figure 5 presents the results for a high-density region without envelope. If we compare the results with the LVG results for the same physical conditions [$n(H_2)$ and abundance of SO], we find that the LVG results are acceptable when the $n(H_2)$ and the abundance of SO are small. However, when self-absorption appears, i.e., when the density $n(H_2)$ and the abundance of SO increases (high line opacity), the line intensities for the transitions $2_3$–$1_2$ and $3_4$–$2_3$ are different using both methods. The intensity of the $0_1$–$1_0$ transition is not affected by self-absorption since the line is optically thin in most models, whereas the lines of the other transitions are optically thick. In view of this result, it will be difficult to derive a reasonable value for the abundance of SO in high-density regions from the LVG method due to these self-absorption effects. Nevertheless, for the typical densities of dark clouds these transitions are not affected by self-absorption because the involved energy levels are not efficiently populated and, hence, their line opacities will be below 1.

Figure 6 presents the results obtained for a low-density region, i.e., the envelope. Here the lines are not affected by self-absorption except for the case of high SO abundance. The results obtained with the Monte Carlo models are consistent with those of the LVG since the opacity of all lines is small. Hence, contrary to

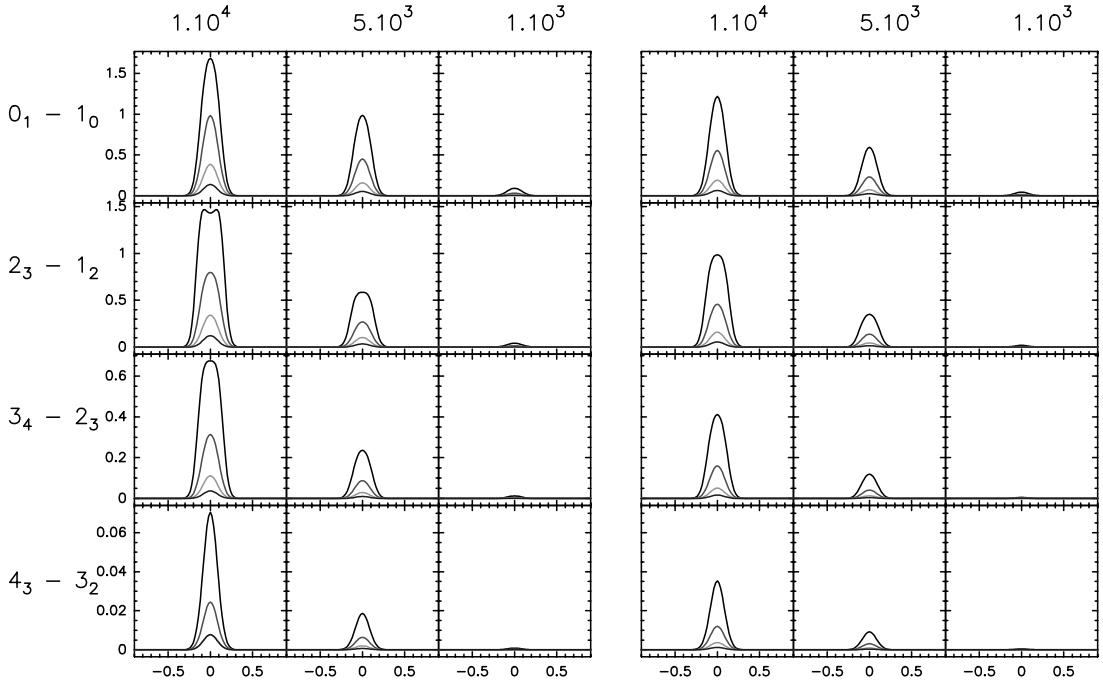


FIG. 6.—Line profiles for different SO transitions obtained with the nonlocal radiative transfer method described in the text. The cloud consists of a low-density region (envelope) with a diameter of 160″ (*left*) and 80″ (*right*). Density is indicated above the panels. The cloud is placed at 140 pc. The SO abundance varies from $10^{-8}$ to $3.3 \times 10^{-10}$ in steps of $1/(10)^{1/2}$. [*See the electronic edition of the Journal for a color version of this figure.*]

high-density regions, observations of low-density regions could be analyzed with the less CPU time consuming LVG method to obtain a reasonable estimation of $n(H_2)$ and $N$(SO) if two or three lines of SO are observed.

Figure 7 presents a model for a core/envelope cloud with a core density of $5 \times 10^4$ cm$^{-3}$. This figure shows that the density of $H_2$ in the envelope has only little influence on the emergent line profiles for low SO abundances, i.e., for optically thin lines. On the other hand, as could be expected, self-absorption appears for the optically thick lines $2_3$–$1_2$ and $3_4$–$2_3$. This effect increases with the density and with the size of the envelope (i.e., with the SO column density). These results indicate that in order to interpret

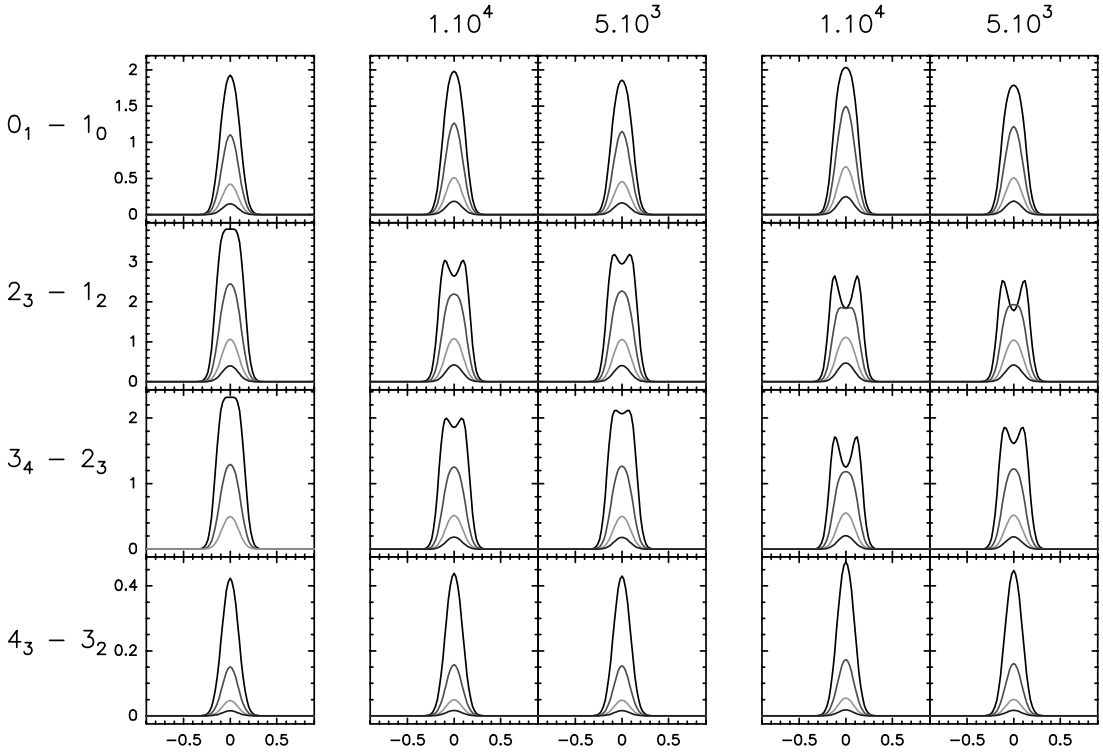


FIG. 7.—Line profiles for different SO transitions obtained with the nonlocal radiative transfer method described in the text. The cloud consists of a high-density region [core, $n(H_2) = 5 \times 10^4$ cm$^{-3}$, $d = 40''$; left plot shows the emerging lines) surrounded by an envelope of diameter 80″ (*middle*) and 160″ (*right*). The density for the envelope is indicated above the panels. The cloud is placed at 140 pc. The SO abundance varies from $10^{-8}$ to $3.3 \times 10^{-10}$ in steps of $1/(10)^{1/2}$. [*See the electronic edition of the Journal for a color version of this figure.*]

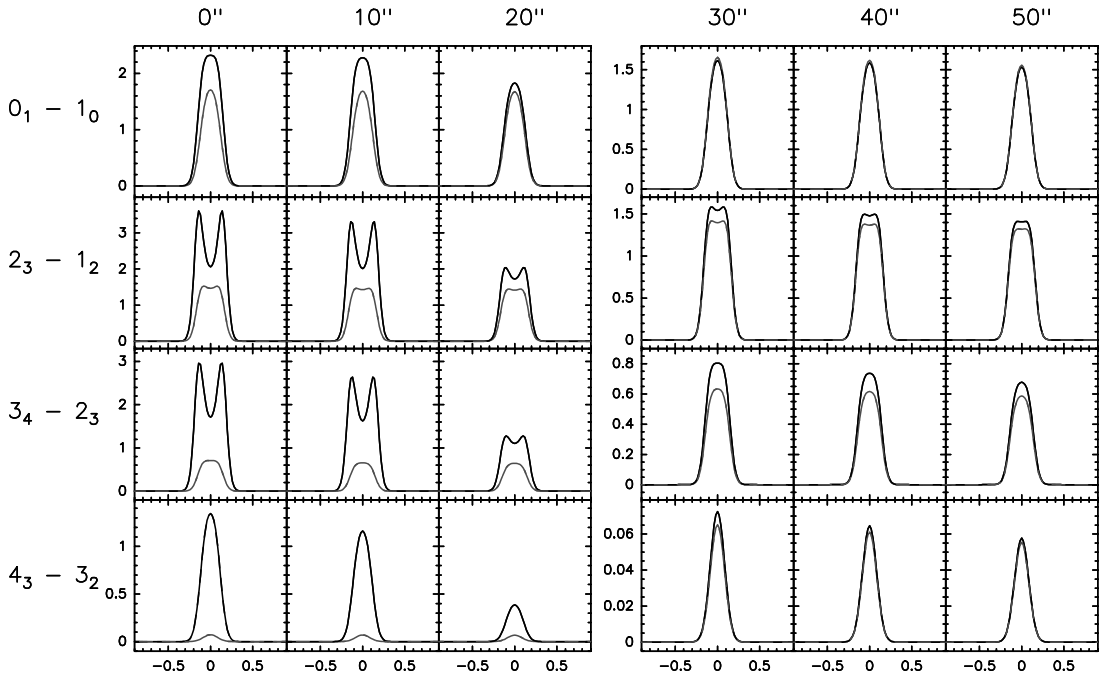


FIG. 8.—Excitation of the envelope by photons coming from the core. The densities of the core and envelope are $10^5$ and $10^4$ cm$^{-3}$, respectively. The diameter of the core is 40″, while that of the envelope is 160″. The abundance of SO is $10^{-8}$. The panels from left to right correspond to different positions in the cloud. For each panel the upper curve corresponds to the emission of the core+envelope and the lower curve to that of the envelope alone. [*See the electronic edition of the Journal for a color version of this figure.*]

the SO line profiles from dense cores surrounded by low density envelopes it will be necessary to use a nonlocal radiative transfer model in order to determine the physical conditions of the gas. However, it is important to note that the $0_1$–$1_0$ and $4_3$–$3_2$ lines are not affected by the presence of an envelope since the opacity of these lines is small in all our models. Several transitions of SO have to be observed in these regions to obtain reliable physical parameters.

We have also studied the radiative pumping of the SO levels in the envelope by the photons coming from the core. Figure 8 shows that this pumping mechanism of the envelope will have little effect on the $0_1$–$1_0$ and $4_3$–$3_2$ lines. The line profiles are the same with or without (*rightmost panels*) the core, a consequence of low opacity of these lines. For the other transitions the pumping of the rotational levels by photons from the core could have some effects on the line intensities as these transitions have large opacities and radiative trapping is important for large SO abundances. However, for the typical densities and SO abundances in dark clouds, the effect is not as important as the one discussed by Cernicharo & Guélin (1987) for $HCO^+$ and by Gonzalez-Alfonso & Cernicharo (1993) for HCN and CS.

Finally, Figure 9 shows the effect of a velocity gradient of 1 km s$^{-1}$ pc$^{-1}$ in the cloud. The core has a density of $2 \times 10^5$ cm$^{-3}$ and a radius of 20″ at 140 pc. The envelope has a radius of 80″ and densities of $10^4$ and $5 \times 10^3$ cm$^{-3}$. The emergent line profiles are very different from those of the static cloud and show important asymmetries. Because of the decoupling by the velocity field of the different regions of the cloud, the lines are stronger than in the static case (in some cases by a factor larger than 1.5). The signature of collapse, i.e., redshifted absorption, appears clearly in most lines, and it is particularly evident in the optically thick ones ($2_3$–$1_2$ and $3_4$–$2_3$). In this case, it is obvious that a nonlocal radiative transfer method has to be used to interpret the observations.

## 3. APPLICATION TO TMC-1

### 3.1. *Observations*

The observations of the $0_1$–$1_0$ line of SO in TMC-1 were carried out with the 100 m Effelsberg telescope. Two maps centered in the ammonia and cyanopolyynes peaks were obtained. The

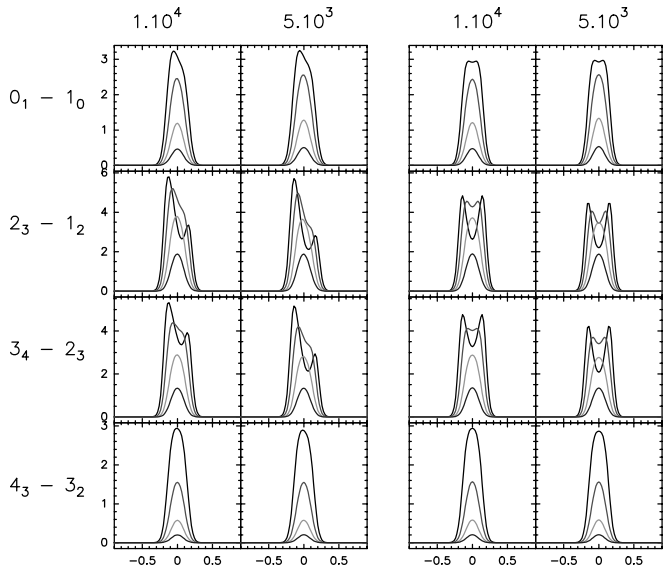


FIG. 9.—Line profiles for different SO transitions obtained with the nonlocal radiative transfer method described in the text. The cloud consists of a high-density region [core, $n(H_2) = 2 \times 10^5$ cm$^{-3}$, $d = 40''$] surrounded by an envelope of diameter 160″ with a velocity gradient of 1 km s$^{-1}$ pc$^{-1}$ (*left*) and without velocity gradient (*right*). The density for the envelope is indicated above the panels. The cloud is placed at 140 pc. The SO abundance varies from $10^{-8}$ to $3.3 \times 10^{-10}$ in steps of $1/(10)^{1/2}$. [*See the electronic edition of the Journal for a color version of this figure.*]

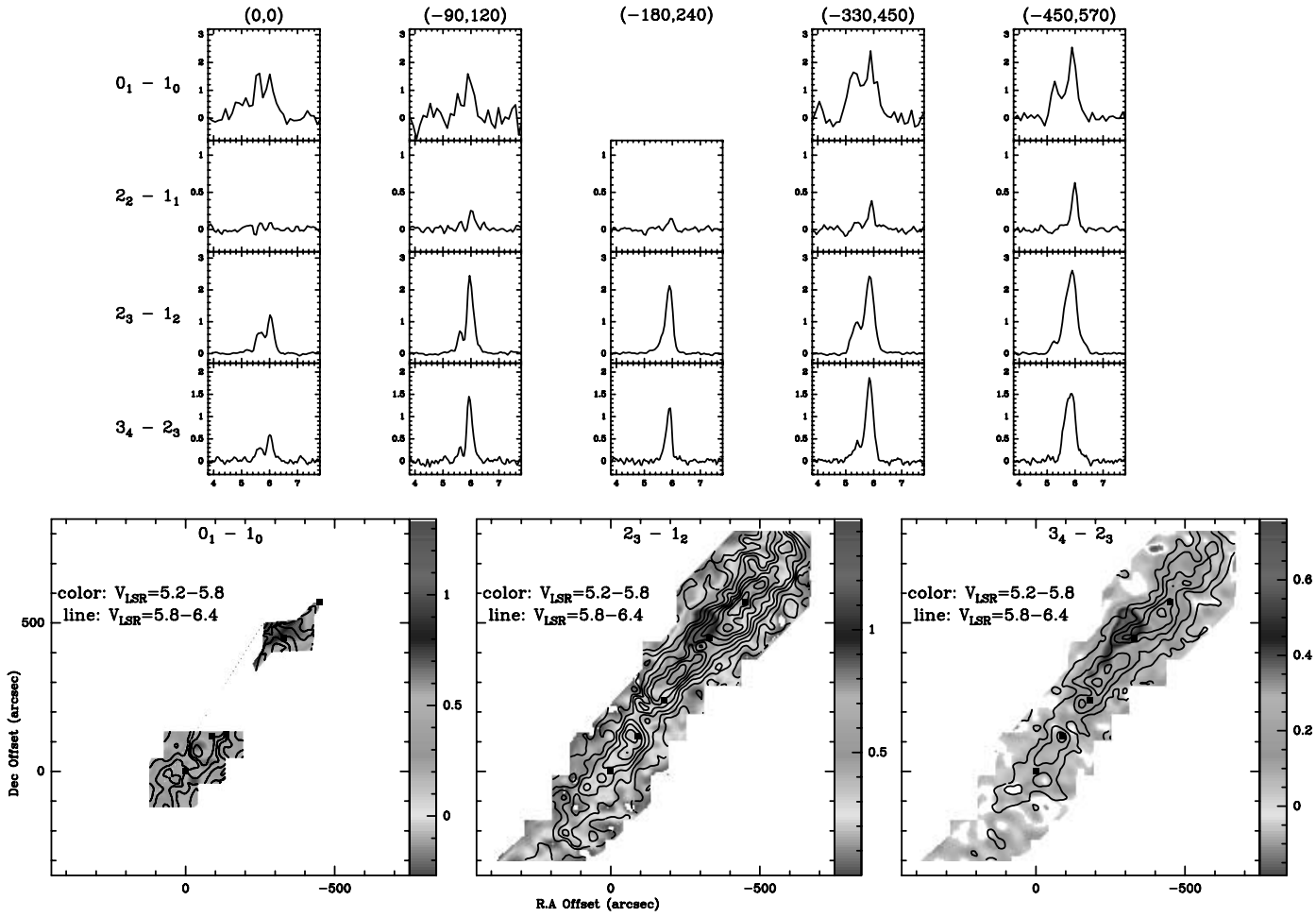


FIG. 10.—Different SO lines observed at selected positions (*top*), and integrated intensity map for the $0_1-1_0$, $2_3-1_2$, and $3_4-2_3$ transitions. The $v_{LSR}$ values are in km s$^{-1}$. [*See the electronic edition of the Journal for a color version of this figure.*]

line of the $^{34}$SO isotope was observed at selected positions but the line detected was very weak. Pointing and focus were done on nearby strong radio continuum sources, whereas the calibration was based on observation of NGC 7027. The velocity resolution of the observations is 0.05 km s$^{-1}$.

The $2_3-1_2$, $3_4-2_3$, and $2_2-1_1$ lines of SO were observed with the 30 m IRAM radio telescope. The first two lines were mapped in a large area covering the entire TMC-1 cloud, whereas the last line was observed at only selected positions. Position switching was used for all observations. An autocorrelator provided a spectral resolution of 0.04–0.1 km s$^{-1}$. The calibration was based on the observation of two absorbers at different temperatures and the ATM code developed by Cernicharo (1985) and updated recently by Pardo et al. (2001). Pointing was checked every hour on CRL 618 and focus was monitored every 2–3 hr on Mars and other planets.

Figure 10 shows the observed lines at selected positions in TMC-1 and the SO integrated intensity maps of the $0_1-1_0$, $2_3-1_2$, and $3_4-2_3$ lines.

### 3.2. *Physical Conditions*

The SO line profiles observed in the present study do not seem to display deep absorption. However, we can clearly see multiple velocity components. This result is not surprising since TMC-1 is well known to have a complex velocity structure. Table 1 presents the velocity components found through Gaussian fits to the observed data at selected positions. For all observed positions the component at $v_{LSR} = 5.8-6.0$ km s$^{-1}$ is stronger than the others. This result is consistent with the previous studies by Rydbeck et al. (1980), who observed the SO $0_1-1_0$ line and showed that the line shapes are not reproduced by a single Gaussian. Although our observations show that the low $v_{LSR}$ component decreases in intensity with increasing upper energy levels, which could be interpreted as self-absorption, we believe (see below) that this effect can be explained by a small volume density for this velocity component. The velocity components seen in SO have been found in several molecules, e.g., OH by Harju et al. (2000) and even in the high rotational level transitions ($J = 9-8$) of $HC_3N$ (Schloerb et al. 1983). Hence, we can be confident in our interpretation of the observed SO lines in TMC-1 in terms of velocity structure.

TABLE 1

$v_{LSR}$ OF THE CLOUD AT DIFFERENT POSITIONS

| Position (arcsec) | Components of $v_{LSR}$ (km s$^{-1}$) |
|---|---|
| (0, 0) | 5.6, 6.0 |
| (−90, 120) | 5.5, 5.9 |
| (−180, 240) | 5.8 |
| (−330, 450) | 5.3, 5.7, 5.9 |
| (−450, 570) | 5.2, 5.6, 5.9 |

This interpretation is opposite to the one by Hirahara et al. (1995) who found that their observations of the SO $2_3$–$1_2$ transition do not reflect multiple velocity components but just self-absorption. The different line profiles from their data and those of Rydbeck et al. (1980) were explained by Hirahara et al. (1995) as a result of the different upper energy level of the two transitions (9.4 K for the $N_J = 2_3$ level compared to 1.4 K for $N_J = 0_1$ level). Hence, for Hirahara et al. (1995) the observed line of Rydbeck et al. (1980) was just showing self-absorption and not multiple velocity components.

Figure 10 shows the integrated intensity maps of the SO lines. They all peak in the northwest region of the TMC-1 ridge, extending further away from the ammonia peak. The lines are, however, weak in the southeast region where cyanopolyynes and other carbon chains are very abundant. These results are consistent with the findings of Hirahara et al. (1995). The integrated line intensity for the two velocity intervals $v_{\rm LSR} = 5.2$–$5.8$ km s$^{-1}$ and $v_{\rm LSR} = 5.8$–$6.4$ km s$^{-1}$ shows a complex structure in the distribution of SO emission in TMC-1 (see Fig. 10), indicating that both velocity ranges are overlapping over the whole cloud, even in regions of low density (the envelope of TMC-1). It would be difficult to explain such behavior by pure line self-absorption.

In order to model the SO emission in TMC-1 and to derive the volume density and the SO abundance, we have used the observed line profiles of the transitions $0_1$–$1_0$, $2_3$–$1_2$, $3_4$–$2_3$, and $2_2$–$1_1$ and applied the LVG and the nonlocal radiative transfer code described previously. We have chosen five positions along the ridge of the cloud, (0, 0), ($-90''$, $120''$), ($-180''$, $240''$), ($-330''$, $450''$), and ($-450''$, $570''$), where our data have the highest signal-to-noise ratio. We have tried to reproduce the line profiles at and around these positions by allowing the temperature, volume density, cloud structure, and column density of SO to vary around the expected values established by previous observations.

We have first analyzed the observations with the LVG code. For all positions it was not possible to reproduce the observed line intensities. Indeed, the intensity of the $0_1$–$1_0$ transition is too important compared to the other transitions and we have been unable to find a set of physical conditions, $T_K$, $n(\rm H_2)$, and $N$(SO), to reproduce the observations. Figure 4 shows that it is not possible with the LVG code to have comparable line intensities for the $0_1$–$1_0$ and $2_3$–$1_2$ transitions, and a line intensity for the $0_1$–$1_0$ transition twice that for the $3_4$–$2_3$ one for $T_K \approx 10$ K, i.e., the kinetic temperature of TMC-1. The difficulties of the LVG analysis indicate that an adequate model should include both a core and an envelope. An important fraction of the intensity of the $0_1$–$1_0$ line could be due to emission in the low-density envelope, whereas the intensity of the other lines are essentially due to the core region. This kind of interpretation is in agreement with models from other authors (Avery et al. 1982; Bujarrabal et al. 1981; Cernicharo & Guélin 1987).

Our nonlocal radiative transfer code is for spherical or plane-parallel geometries. However, the geometry of TMC-1 seems to be cylindric, as indicated by Figure 10 (see also Avery et al. 1982). We have modeled the cloud by summing several different spherical components, expecting that the results will not be really different from those of a cylindric geometry. The very low intensity of the transition $2_2$–$1_1$ is the signature of a moderate-density core. We have taken a temperature of 10 K in the envelope since this part of the cloud is a low density region that does not contribute to the $2_2$–$1_1$ line emission. Different runs indicate that for the core a temperature of 8 K is better adapted to the interpretation of the SO lines, in particular, of the $2_2$–$1_1$ transition. We have well reproduced the observations with the parameters given by Figure 11. The simulated and observed spectra are presented in Figure 12.

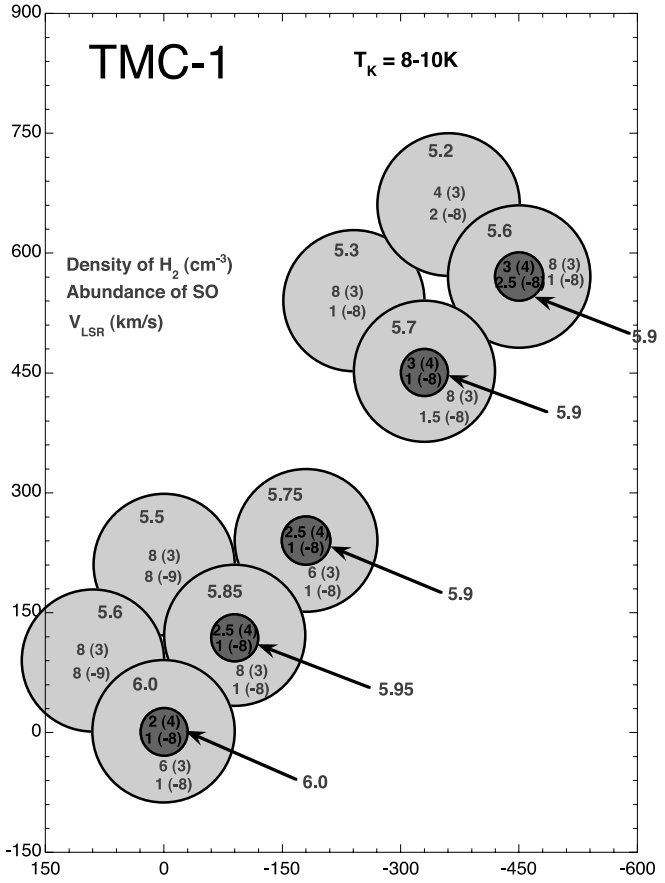


FIG. 11.—Model for TMC-1. [*See the electronic edition of the Journal for a color version of this figure.*]

We have modeled the region near the cyanopolyyne peak by a cloud model constituted by a core [$n(\rm H_2) = 2 \times 10^4$ cm$^{-3}$] and an envelope [$n(\rm H_2) = 6 \times 10^3$ cm$^{-3}$] at the same $v_{\rm LSR}$ (5.9–6.0 km s$^{-1}$). The SO abundance in both components is $10^{-8}$. A third component, with a lower volume density, $n(\rm H_2) = 8 \times 10^3$ cm$^{-3}$, and shifted $45''$ to the northeast at smaller $v_{\rm LSR}$ (5.6 km s$^{-1}$) was necessary to fit the spatial distribution of the observed SO lines and their intensities. This component is mainly required by the $0_1$–$1_0$ transition, which has an intensity peak at this position. The other lines are weak, which implies a moderate density. The derived SO abundance is $8 \times 10^{-9}$. The two other positions close to the cyanopolyyne peak give similar densities and SO abundances. The third velocity component is also needed around ($-90''$, $120''$).

For the other region, near the ammonia peak, we have tried to reproduce the observations with a similar model, but we fail to obtain a good fit for all SO lines. This is due to the fact that the intensity and the shape of the lines $0_1$–$1_0$, $2_3$–$1_2$, and $3_4$–$2_3$ are strongly asymmetric compared to the $2_2$–$1_1$ line. These lines seem to be slightly shifted compared to line $2_2$–$1_1$, suggesting that the envelope is not at the same $v_{\rm LSR}$ than the core but at a slightly smaller $v_{\rm LSR}$. Taking into account all the above remarks, we have built a model with the parameters given in Figure 11. The cloud is constituted by a core region with a temperature of 8 K and at a velocity of $v_{\rm LSR} = 5.9$ km s$^{-1}$ and by an envelope at $v_{\rm LSR}$ of 5.6–5.7 km s$^{-1}$ with a temperature of 10 K. Another component with a low $\rm H_2$ density [$(4$–$8) \times 10^3$ cm$^{-3}$ at 10 K] and

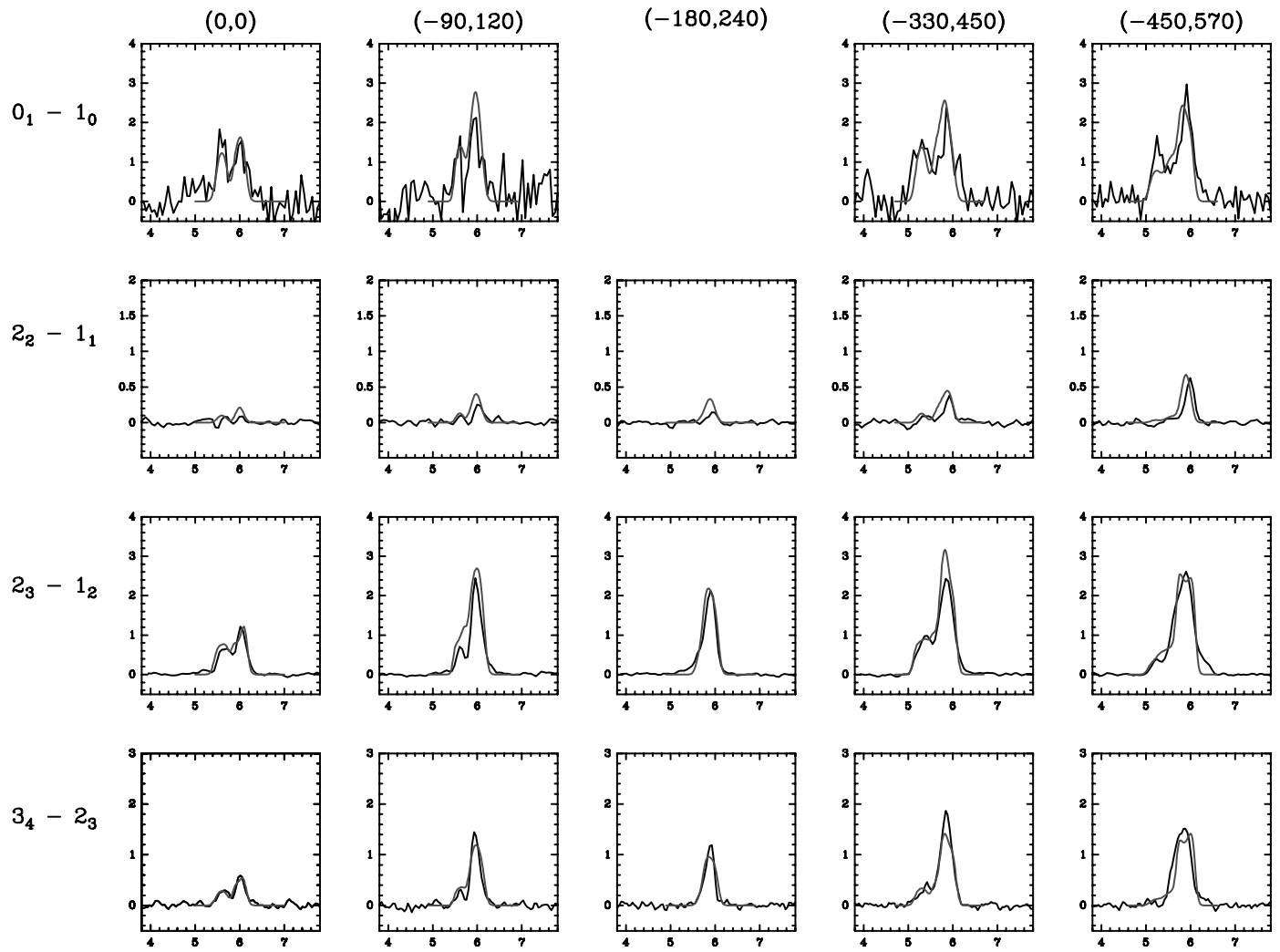


FIG. 12.—Theoretical line profile compared to observations at selected positions. [*See the electronic edition of the Journal for a color version of this figure.*]

$v_{LSR} = 5.2–5.3$ km s$^{-1}$ was also included. It was slightly shifted to the northeast for the same reason as near the cyanopolyyne peak. With this model, we have well reproduced the observed spectra (see Fig. 12). $^{34}$SO has also been detected in TMC-1, but the line is too weak to allow any reliable determination of the abundance of SO to be made, taking into account the fact that the abundance of $^{34}$SO is nearly 20 times lower than the abundance of $^{32}$SO (Pratap et al. 1997). Nevertheless, the upper limits on its emission have been used to provide additional constraints on the column density of SO.

### 3.3. *Analysis and Discussion*

The results obtained from our models for TMC-1 differ from those by other authors for the density of $H_2$ and for abundance of SO. Only the temperature parameter of the cloud is found in good agreement with the temperatures obtained in previous studies (8–10 K). We have found an $H_2$ density lower than other authors (Pratap et al. 1997; Avery et al. 1982; Schloerb et al. 1983; Hirahara et al. 1995). This can be explained first by the fact that some of the observed transitions in this work involve relatively high SO energy rotational levels that have not been observed in previous works. The lack of emission from these high energy levels of SO introduces a strong constraint on the density. The differences can also be explained by the cloud structure adopted. Models that do not use a core and an envelope region (Pratap et al. 1997; Schloerb et al. 1983) have generally found a volume density higher than that obtained in our models. This is related to how the envelope affects each line since it produces a decrease of the line intensity for transitions involving low energy levels without affecting those arising from high energy levels. Hence, an incorrect modeling of the cloud structure leads to an overestimate of the density. The density that we have found is in good agreement with that determined by Gaida et al. (1984), Bujarrabal et al. (1981), and Rydbeck et al. (1980), who modeled the cloud in a similar way to ours. The differences between the core density in our model and those of Avery et al. (1982) are probably due to the use of lines from different molecular species (SO and $HC_3N$) having different excitation conditions and probably different chemistries. SO is preferentially formed by S + OH and S + $O_2$ reactions so, as shown by Turner (1995) and Charnley (1997), the sulfur chemistry is linked to oxygen chemistry. Indeed, SO is more abundant in O-rich regions whereas the carbon chain molecules (such as $HC_3N$) are formed through ion-neutral reactions (see Fukuzawa & Osamura 1997). Hence, SO and $HC_3N$ abundances could depend on different chemical paths. Small differences in the electron abundance could affect the abundance of molecules formed through ion-neutral reactions (see Fossé et al. 2001). It could also be possible that our densities reflect an

averaged density for a core with a high density gradient. However, the lack of emission from high energy levels of SO indicates that if there are regions in the core with higher densities than those found in our models, they have to be strongly diluted in the beam of the 30 m radio telescope or else the SO is strongly depleted in dense regions.

The densities, or average densities, that we have obtained for the cores along TMC-1 do not change significantly with position. The abundance of SO found in this cloud is lower than in previous works (Pratap et al. 1997; Hirahara et al. 1995). This can be explain by two reasons:

1. The use of the new rate coefficients that are higher than those of G94 used in previous works. As we have seen in § 2.2, the use of the G94 rate coefficients can induce an error of a factor 2–10 in the determination of the abundance of SO.
2. Pratap et al. (1997) and Hirahara et al. (1995) used an LVG code for the determination of the density column and have reproduced only one line (Hirahara et al. 1995), or lines at nearly all the same frequency (Pratap et al. 1997). Consequently, $N$(SO) is not as well constrained by these data and the simple LVG analysis as it is with the greater number of transitions used in this paper and the Monte Carlo models.

We have found that the abundance of SO is practically constant along the TMC-1 ridge, $X(\mathrm{SO}) \simeq 10^{-8}$, except at the position of the ammonia peak (−450, 570), where it reaches $X(\mathrm{SO}) = 2.5 \times 10^{-8}$.

Our model contains different velocity structures for the different cores and their envelopes: the $v_{\mathrm{LSR}}$ of the core seems to be higher than the $v_{\mathrm{LSR}}$ of the envelope near the ammonia peak. This complex velocity structure has been already found for this cloud by Snell et al. (1982) and Hirahara et al. (1992) from observations of CS and carbon chain molecules, respectively. Snell et al. (1982) and Hirahara et al. (1992) have published models for TMC-1, and our study in terms of velocity structure, although not exactly the same, is consistent with their results. Hence, we have different $v_{\mathrm{LSR}}$ values for the ridge and it seems that the velocity component at 5.2–5.3 km s$^{-1}$ for the ammonia peak region is due to a part of the cloud that is not centered on the ridge. This is shown by the fact that the line intensity at these velocities does not decrease when we move perpendicularly to the ridge but increases and presents an intensity maximum northeast of the ridge. A similar behavior is found for the component at 5.6 km s$^{-1}$ near the cyanopolyyne peak.

The velocity structure depicted in Figure 10 suggests that the two main velocity components in TMC-1 are physically associated and do not result from a chance alignment of two clouds in the line of sight. The red component, $v_{\mathrm{LSR}} = 5.8$–$6.4$ km s$^{-1}$, peaks slightly west of the blue one, $v_{\mathrm{LSR}} = 5.2$–$5.8$ km s$^{-1}$, around the ammonia peak but becomes coincident at positions around (−500″, 600″) and (−250″, 350″). Toward the south, the red component is stronger and slightly shifted to the east around the cyanopolyyne peak. Both velocity components coexist along the TMC-1 ridge, and their spatial distribution probably represents the gravitational interaction between the low/moderate density envelopes around the different cores, and the cores themselves. It is worth noting that the observed velocity structure could be interpreted as that of a truncated cylindrical shell expanding at 0.3 km s$^{-1}$ with a central $v_{\mathrm{LSR}}$ of 5.6 km s$^{-1}$. This shell is placed at the edge of the long filament containing TMC-1 and TMC-1C (Cernicharo et al. 1984; Cernicharo & Guélin 1987) as it is submitted to a large UV field. Important differences have been found in TMC-1 for the abundance of cyclic and linear carbon chains as a function of the position perpendicular to the TMC-1 ridge, suggesting that the different parts of the filament are submitted to different chemical processes such as different UV fields or visual absorption across the shell (Fossé et al. 2001). The observed shell structure and its velocity field could also reflect the remnant of the interaction in the past of the bipolar outflow emerging from the class I source 04381+2540, a source that is located at (0″, −270″) of the ammonia peak (Hirahara et al. 1992). Although speculative, this hypothesis is not unlikely as bipolar outflows have energy and momentum enough to modify the physical structure of the surrounding quiescent gas (see Bachiller 1996; Cernicharo & Reipurth 1996).

Finally, we have found a spatial distribution of the SO molecule similar to the distribution of other sulfur-bearing species present in the cloud such as CS (Snell et al. 1982) and $H_2S$ (Minh et al. 1989). The emission peak of SO is in the direction of the ammonia source. The abundance of SO decreases smoothly from this peak toward the southeast. This result is not surprising since the sulfur is originally contained in $H_2S$ and reacts respectively with CO and OH molecules to give CS and SO. The spatial distribution of SO is also similar to CO, $N_2H^+$, and $NH_3$ but differs from the carbon chain molecules (Hirahara et al. 1992; Bujarrabal et al. 1981) that are mainly localized at the cyanopolyyne peak.

## 4. CONCLUSIONS

In this paper, we have studied the impact of new collisional rate coefficients for the system SO-He on the interpretation of observations of cold dark clouds. Compared to previously published calculations by G94, the new results on SO appear to be more robust, providing better diagnostics to derive the physical conditions of cold molecular clouds. In particular, the G94 rates could result in overestimating the density or column density in cold molecular clouds. The new rates were used to reexamine the physical conditions and the abundance of SO in the cold dark cloud TMC-1 by using mapping results in the low-lying transitions of SO. The structure of TMC-1 is well described by a cylindric filament containing several cores [$T_K = 8$ K, $n(\mathrm{H_2}) \sim 3 \times 10^4$ cm$^{-3}$] along the ridge and an envelope [$T_K = 10$ K, $n(\mathrm{H_2}) \sim (6$–$8) \times 10^3$ cm$^{-3}$] surrounding these condensations. The abundance of SO in TMC-1 is nearly constant throughout the cloud: $10^{-8}$, except at the ammonia peak where the abundance reaches $2.5 \times 10^{-8}$. The velocity structure of TMC-1 suggests that the envelope and the cores are physically associated and do not result from a chance alignment of different clouds. Although it is difficult to find a geometrical and velocity model for TMC-1, we found that a truncated cylindrical shell expanding at 0.3 km s$^{-1}$ placed at the edge of one of the main filaments of HCL-2 (see Cernicharo & Guélin 1987) could fit the observed velocity structure.

We would like to acknowledge N. Feautrier and A. Spielfiedel for their continuing interest in this work. We acknowledge the financial support of the PAI PICASSO and of the Spanish MEC grants AYA2003-2785, AYA2002-10113-E, and ESP2004-00665. This study is supported in part by the European Community's Human Potential Programme under contract MCRTN 512302, Molecular Universe.

REFERENCES

Avery, L. W., MacLeod, J. M., & Broten, N. W. 1982, ApJ, 254, 116
Bachiller, R. 1996, ARA&A, 34, 111
Bernes, C. 1979, A&A, 73, 67
Blake, G. A., Sutton, E. C., Masson, C. R., & Phillips, T. G. 1987, ApJ, 315, 621
Blake, G. A., van Dishoeck, E. F., Jansen, D. J., Groesbeck, T., & Mundy, L. G. 1994, ApJ, 428, 680
Bujarrabal, V., Guélin, M., Morris, M., & Thaddeus, P. 1981, A&A, 99, 239
Castor, J. I. 1970, MNRAS, 149, 111
Cernicharo, J. 1985, ATM: A Program to Compute Atmospheric Absorption up to 1 THz (internal rep.; Granada: IRAM)
Cernicharo, J., & Guélin, M. 1987, A&A, 176, 299
Cernicharo, J., Guélin, M., & Askne, J. 1984, A&A, 138, 371
Cernicharo, J., & Reipurth, B. 1996, ApJ, 460, L57
Charnley, S. B. 1997, ApJ, 481, 396
Fossé, D., Cernicharo, J., Gerin, M., & Cox, P. 2001, ApJ, 552, 168
Fukuzawa, K., & Osamura, Y. 1997, ApJ, 489, 113
Gaida, M., Ungerechts, H., & Winnewisser, G. 1984, A&A, 137, 17
Goldreich, P., & Kwan, J. 1974, ApJ, 189, 441
Gonzalez-Alfonso, E., & Cernicharo, J. 1993, A&A, 279, 506
Gottlieb, C. A., & Ball, J. A. 1973, ApJ, 184, L59
Green, S. 1994, ApJ, 434, 188 (G94)
Green, S., & Chapman, S. 1978, ApJS, 37, 169
Green, S., & Thaddeus, P. 1976, ApJ, 205, 766
Harju, J., Winnberg, A., & Wouterloot, J. G. A. 2000, A&A, 353, 1065
Hirahara, Y., et al. 1992, ApJ, 394, 539
———. 1995, PASJ, 47, 845
Lique, F., Spielfiedel, A., & Cernicharo, J. 2006, A&A, 451, 1125
Lique, F., Spielfiedel, A., Dubernet, M.-L., & Feautrier, N. 2005, J. Chem. Phys., 123, 134316 (L05)
Minh, Y. C., Irvine, W. M., & Ziurys, L. M. 1989, ApJ, 345, L63
Morris, M., Turner, B. E., Palmer, P., & Zuckerman, B. 1976, ApJ, 205, 82
Pardo, J. R., Cernicharo, J., & Serabyn, G. 2001, IEEE Trans. Antennas and Propagation, 49, 1683
Pineau des Forêts, G., Roueff, E., Schilke, P., & Flower, D. R. 1993, MNRAS, 262, 915
Pratap, P., Dickens, J. E., Snell, R. L., Miralles, M. P., Bergin, E. A., Irvine, W. M., & Schloerb, F. P. 1997, ApJ, 486, 862
Rydbeck, O. E. H., Irvine, W. M., Hjalmarson, A., Rydbeck, G., Ellder, J., & Kollberg, E. 1980, ApJ, 235, L171
Schloerb, F. P., Snell, R. L., & Young, J. S. 1983, ApJ, 267, 163
Snell, R. L., Langer, W. D., & Frerking, M. A. 1982, ApJ, 255, 149
Sobolev, V. V. 1958, Theoretical Astrophysics, ed. V. A. Ambartsumyan (London: Pergamon Press), chap. 29
———. 1960, Moving Envelopes of Stars (Cambridge: Harvard Univ. Press)
Turner, B. E. 1995, ApJ, 455, 556
Turner, B. E., Chan, K.-W., Green, S., & Lubowich, D. A. 1992, ApJ, 399, 114
van Dishoeck, E. F., Jansen, D. J., & Phillips, T. G. 1993, A&A, 279, 541